# Gliding motility of *Plasmodium* merozoites

Kazuhide Yahata[a,b,1,2], Melissa N. Hart[c,1], Heledd Davies[b], Masahito Asada[a,d], Samuel C. Wassmer[c], Thomas J. Templeton[a], Moritz Treeck[b], Robert W. Moon[c,2], and Osamu Kaneko[a]

[a]Department of Protozoology, Institute of Tropical Medicine (NEKKEN), Nagasaki University, 1-12-4 Sakamoto, Nagasaki 852-8523, Japan; [b]Signalling in Apicomplexan Parasites Laboratory, The Francis Crick Institute, London NW1 1AT, United Kingdom; [c]Faculty of Infectious and Tropical Diseases, London School of Hygiene & Tropical Medicine, London WC1E 7HT, United Kingdom; and [d]National Research Center for Protozoan Diseases, Obihiro University of Agriculture and Veterinary Medicine, Nishi 2-11, Obihiro, Hokkaido 080-0834, Japan

*Plasmodium* malaria parasites are obligate intracellular protozoans that use a unique form of locomotion, termed gliding motility, to move through host tissues and invade cells. The process is substrate dependent and powered by an actomyosin motor that drives the posterior translocation of extracellular adhesins which, in turn, propel the parasite forward. Gliding motility is essential for tissue translocation in the sporozoite and ookinete stages; however, the short-lived erythrocyte-invading merozoite stage has never been observed to undergo gliding movement. Here we show *Plasmodium* merozoites possess the ability to undergo gliding motility in vitro and that this mechanism is likely an important precursor step for successful parasite invasion. We demonstrate that two human infective species, *Plasmodium falciparum* and *Plasmodium knowlesi*, have distinct merozoite motility profiles which may reflect distinct invasion strategies. Additionally, we develop and validate a higher throughput assay to evaluate the effects of genetic and pharmacological perturbations on both the molecular motor and the complex signaling cascade that regulates motility in merozoites. The discovery of merozoite motility provides a model to study the glideosome and adds a dimension for work aiming to develop treatments targeting the blood stage invasion pathways.

malaria | plasmodium | merozoite | gliding | invasion

Apicomplexan parasites traverse tissues and invade cells via a mechanism known as gliding motility, a process unique to the phylum that uses neither propulsive structures such as flagella or cilia, nor cellular shape changes as for peristaltic and amoeboid motility (1, 2). Motility of invasive forms of malarial parasites (termed "zoites") was first described for the ookinete stage in avian blood (3), and then for the sporozoite stage in the mosquito (4, 5). Unlike ookinetes and sporozoites, which must traverse through tissues, no gliding motility has been described for the merozoite, which invades erythrocytes in the bloodstream. Instead, only limited reorientation movement and cellular deformation has been observed across several malarial parasite species, including *Plasmodium knowlesi*, *Plasmodium falciparum*, and *Plasmodium yoelii* (6–8). Due to frequent and passive encounters with erythrocytes in the bloodstream shortly after egress, it has been presumed that merozoites do not require motility, leading to the consensus that the molecular motor is principally required for entry into the erythrocyte (9).

Gliding has perhaps been best described for *Toxoplasma gondii* tachyzoites and *Plasmodium berghei* sporozoites, both of which exhibit helical motion in three-dimensional (3D) matrices, as well as during host cell entry, that is driven by an actomyosin motor (10–12). Components of this motor, collectively called the "glideosome," are located within the space between the parasite inner membrane complex (IMC) and plasma membrane; they are generally conserved between apicomplexan zoites, including merozoites (11, 13, 14). According to the linear motor model, gliding is a substrate-dependent process. Transmembrane ligands are secreted from organelles called micronemes at the apical end of the zoite, where they bind to

receptors on the surface of the host cell or tissue via their ectodomains, while also connecting to the actomyosin motor through their cytoplasmic tails (11). MyoA engagement with actin subsequently pulls both actin and the receptor-bound ligand rearward, thereby driving the zoite forward. Finally, the ectodomains of receptor-bound ligands are cleaved by parasite-derived proteases, thus disengaging them from their host cell receptors (11). Deletion of key motor components, including myosin A (MyoA) (15), actin-1 (ACT1) (16), and glideosome-associated protein 45 (GAP45) (17), prevent *P. falciparum* merozoites from invading host erythrocytes, demonstrating the essentiality of the actomyosin motor for erythrocyte invasion (9).

Here we show that both *P. falciparum* and *P. knowlesi* merozoites are capable of gliding motility across both erythrocyte surfaces and polymer coverslips and that motility modulates multiple steps of invasion. We developed an assay to evaluate the effect of genetic and pharmacological perturbations on both the molecular motor and the complex signaling cascade that regulates motility in merozoites.

## Results

**Gliding Motility of *Plasmodium* Merozoites.** Here we sought to address the long-standing theory that malarial merozoites do

**Significance**

*Plasmodium* malaria parasites use a unique substrate-dependent locomotion, termed gliding motility, to migrate through tissues and invade cells. Previously, it was thought that the small labile invasive stages that invade erythrocytes, merozoites, use this motility solely to penetrate target erythrocytes. Here we reveal that merozoites use gliding motility for translocation across host cells prior to invasion. This forms an important preinvasion step that is powered by a conserved actomyosin motor and is regulated by a complex signaling pathway. This work broadens our understanding of the role of gliding motility and invasion in the blood and will have a significant impact on our understanding of blood stage host–pathogen interactions and parasite biology, with implications for interventions targeting erythrocyte invasion.

[1]K.Y. and M.N.H. contributed equally to this work.

[2]To whom correspondence may be addressed. Email: kyahata@nagasaki-u.ac.jp or rob.moon@lshtm.ac.uk.

MICROBIOLOGY

not undergo conventional gliding motility. While motility of sporozoites is normally observed on bovine serum albumin (BSA)-coated glass slides, merozoites do not glide on this substrate. However, when using polymer coverslips with a hydrophilic coating (ibiTreat), we observed motile merozoites. When imaged immediately after erythrocyte egress, *P. falciparum* merozoites show directional movement on the coverslip surface which displaces them from the hemozoin-containing residual body (Fig. 1 and Movies S1 and S2). The average *P. falciparum* merozoite gliding speed was 0.6 μm/s (SD = 0.14 μm/s; $n = 10$ individual merozoites), considerably slower than that of *P. yoelii* sporozoites (helical gliding 5.0 μm/s; SD = 0.83 μm/s; $n = 8$) and *P. berghei* sporozoites (2 μm/s to 3 μm/s) (18), *Toxoplasma gondii* tachyzoites (helical gliding 2.6 μm/s; SD = 0.54 μm/s; $n = 13$; circular gliding 1.8 μm/s; SD = 0.32 μm/s; $n = 13$), and *Babesia bovis* merozoites (6.0 μm/s; SD = 0.73 μm/s; $n = 5$), but significantly faster than *P. berghei* ookinetes (helical gliding 5.8 μm/min) (19). The longest gliding time of *P. falciparum* merozoites was 43 s, shorter than those of *P. yoelii* sporozoites (>600 s), *T. gondii* tachyzoites (>600 s), and *B. bovis* merozoites (125 s). Thus, the short-lived motility of *P. falciparum* merozoites appears to correlate with their decline in erythrocyte invasion efficiency within a few minutes after egress (20).

The zoonotic malaria parasite, *P. knowlesi,* has much larger and longer-lived merozoites (20–22) and is capable of invading both human and macaque erythrocytes (23); thus, we hypothesized that this may result in different gliding behavior. In the absence of fresh erythrocytes, *P. knowlesi* merozoites also exhibit some motility on ibiTreat coverslips, but the number of motile merozoites increases using Poly-L-lysine–coated (PLL) polymer coverslip surfaces (Movie S3). A median 62% (interquartile range [IQR] = 55%) of all merozoites within a given schizont exhibited motility on PLL-coated coverslips, with a "gliding" merozoite defined as one which attached to the coverslip surface and exhibited forward movement for at least five continuous seconds (Fig. 2*A*). To test whether gliding is surface dependent, *P. knowlesi* merozoites were also monitored on uncoated polymer and glass coverslips. A much lower percentage of motile parasites was observed for the uncoated polymer (mean = 38%; SD = 36%) and glass coverslips (mean = 25%; SD = 22%) (SI Appendix, Fig. S1A). This suggests that both the coating and the use of polymer rather than glass coverslips is critical for optimal gliding to occur and may account for why merozoite motility has not been observed previously.

*P. knowlesi* merozoites were faster (mean = 1.1 μm/s; SD = 0.29 μm/s; $n = 57$ individual merozoites) than *P. falciparum* (SI Appendix, Fig. S1B) and were capable of gliding for up to 316 s (Fig. 2*B*) on PLL surfaces. To assess the involvement of an actomyosin motor for merozoite motility, egressing merozoites were treated with the actin polymerization inhibitor, cytochalasin D (0.1 μM; concentration that inhibits response by 50% [$IC_{50}$] = 23 nM). This treatment completely inhibited motility (Fig. 2*A* and Movie S4). Cytochalasin D addition also prevented efficient dispersal post egress and frequently resulted in merozoites remaining attached to each other and/or the residual body (Fig. 2*A* and Movie S4). However, while dispersal was inhibited, cytochalasin D treatment did not impede egress itself, as visualized using wheat germ agglutinin–stained erythrocytes and *P. knowlesi* schizonts treated with the drug (Movie S4). The capacity for erythrocyte egress is in line with observations of cytochalasin D-treated *P. falciparum* parasites (17) (Movie S4). Even without inhibitors, *P. knowlesi* merozoite movement was sometimes impaired by groups of merozoites remaining attached to each other. Notably, however, in many instances, pairs or smaller groups of merozoites were frequently observed to glide together in unison when "pointing" in the same direction. Merozoites often completed several glides, with a median cumulative distance of 14 μm (IQR = 16 μm) and some traveling as far as 200 μm within the 10-min imaging window (SI Appendix, Fig. S1C). The majority of gliding occurred within 5 min of egress (SI Appendix, Fig. S1D), with peak gliding occurring during the initial 1- to 2-min window. Gliding speed appeared to decline over subsequent glides (SI Appendix, Fig. S1E), indicative of declining motor function over time, which potentially contributes to the window of merozoite viability. No increase in gliding activity was observed when freshly egressed parasites were first incubated in the dark for 5 min prior to commencing imaging for an additional 4 min (SI Appendix, Fig. S1D). Thus, for *P. knowlesi,* continuous light exposure is unlikely to be the cause of declining motor function (SI Appendix, Fig. S1 *D* and *E*).

Like other apicomplexan zoites (10, 24, 25), *P. knowlesi* merozoites appear to undergo corkscrew-like rotation (Movie S5), with a correlation between the number of turns and forward translocation, indicating a link between the two motions (Fig. 2 *C* and *D*). On average, for each body length the merozoite moved forward, it rotated 0.8 times—equivalent to a tangential velocity of 1.0 μm/s ($n = 10$ merozoites). This is consistent with a linear motor running at a 42° angle down the longitudinal axis of the merozoite. Nine out of ten merozoites rotated counterclockwise, demonstrating the same chirality seen for *Plasmodium* ookinetes (26). Rotation could not be discerned for *P. falciparum* merozoites, likely due to the round morphology and small size.

For both *Plasmodium* species, gliding and invasion proceeded with the wider end of the merozoite leading, rather than the narrower pointed end (Fig. 2*D*). The narrower, pointed end has been widely suggested to contain the apical complex of the parasite, and indeed is consistent with early images of invading parasites by transmission electron microscopy (27). To test whether the apical complex is instead located at the wider end of the parasite, we examined *P. knowlesi*
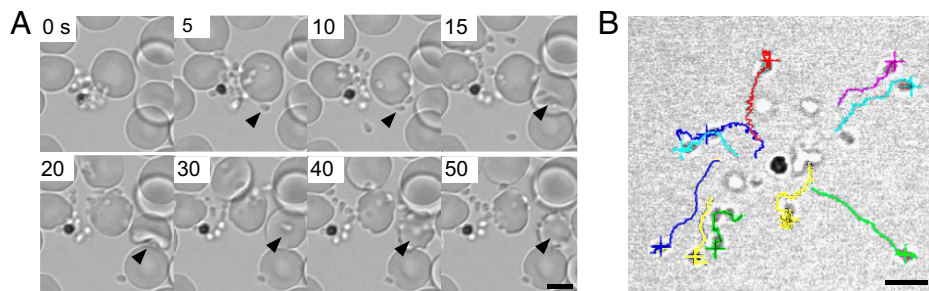


**Fig. 1.** Gliding motility of *P. falciparum* merozoites. (*A*) Time-lapse imaging for *P. falciparum* merozoite gliding motility and erythrocyte invasion. Still images from Movie S1. Arrowhead indicates a merozoite gliding on the coverslip (5 and 10 s), followed by erythrocyte deformation (15 and 20 s) and merozoite internalization (30 s to 50 s). (Scale bar, 5 μm.) (*B*) Each merozoite was traced in different colors, and gliding speed was evaluated from Movie S2. (Scale bar, 5 μm.)
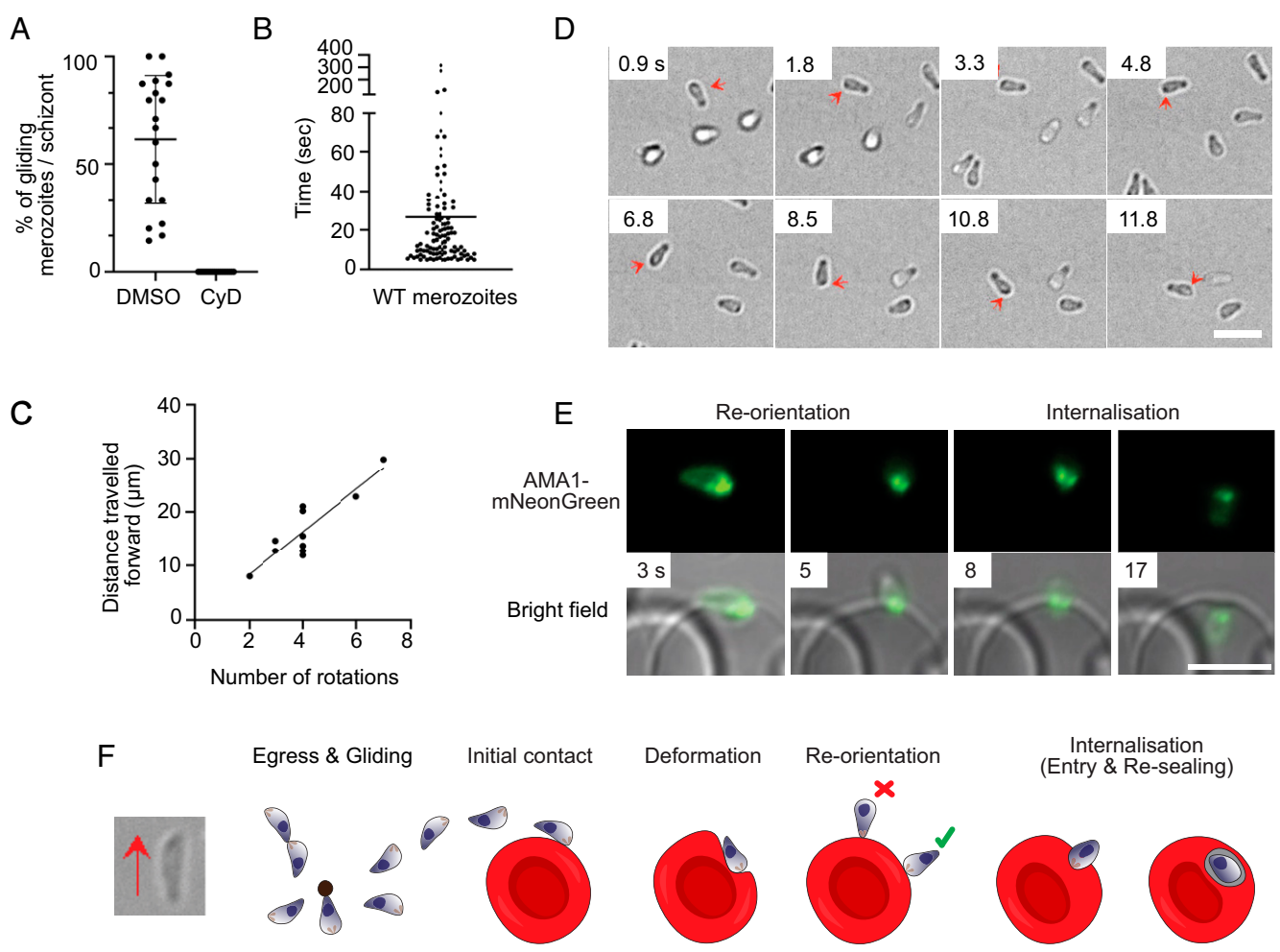
**Fig. 2.** Gliding motility of *P. knowlesi* merozoites. (*A*) The percentage of merozoites within a *P. knowlesi* schizont which exhibit motility, for both DMSO-treated parasites (mean = 62.5%) and 0.1 μM cytochalasin D (CyD; IC$_{50}$ = 0.023 ± 6.7 nM)-treated parasites (no gliding observed). A "motile" merozoite was defined as having demonstrated directional forward motion along the surface of the coverslip for at least five continuous seconds. Each dot is representative of one schizont (*n* = 20). Error bars denote ±1 SD. (*B*) The total time each motile *P. knowlesi* merozoite (*n* = 109; median = 15 s) spent gliding during the 10-min imaging window post egress. Error bars indicate interquartile range. (*C*) Number of rotations that merozoites completed plotted against the distance traveled for each glide (*n* = 10). As the number of rotations increased, so did the distance traveled forward, indicating rotation drives forward motion (Pearson correlation coefficient, *R* = 0.88). (*D*) Time-lapse imaging demonstrating a *P. knowlesi* merozoite rotating as it glides. Red arrows indicate a dark spot located to one side of the wider end of the merozoite, which shifts to the opposite side (shown in subsequent frames), as it turns, and then back to the original position to complete a full rotation (Movie S6). (Scale bar, 5 μm.) (*E*) Time lapse imaging depicting a *P. knowlesi* merozoite with mNeonGreen-tagged AMA1 invading an erythrocyte. *Left* and *Left Center* demonstrate reorientation of the wider end of the merozoite to align with the erythrocyte membrane. This is followed by (*Right Center*) the formation of the moving junction, depicted as two green dots at the merozoite-erythrocyte interface, and, finally, (*Right*) entry into the host cell. (Scale bar, 5 μm.) (*F*) Schematic illustrating gliding and erythrocyte invasion. Gliding proceeds with the wider, apical end of the merozoite leading. During gliding, merozoites stretch, and a pointed protrusion can be seen at the wider end of the zoite (left-hand bright-field image), which engages with the erythrocyte membrane upon reorientation and internalization. Reorientation of the zoite to make a contact of wider end (green tick), and not the thinner end of the zoite as previously hypothesized (red cross), with the erythrocyte membrane occurs prior to entry. During internalization, constriction of the apical end of the zoite causes the basal end to expand. Finally, after entry is complete, the parasite resides in a parasitophorous vacuole where its development continues.

parasites expressing mNeonGreen-tagged apical membrane antigen 1 (AMA1-mNG) using live microscopy. Movie S6 clearly shows that the apical end is located at the wider end of the zoite (Fig. 2*E*), and that host cell entry proceeds in the same orientation as surface gliding, as observed previously for *B. bovis* merozoites (25). Imaging of the AMA1-mNG parasites also shows, using live microscopy to image *Plasmodium* invasion, the formation of a ring structure of the tight junction as the parasite invades the host erythrocyte (Fig. 2*E* and Movie S6). A small protrusion likely corresponding to the apical complex is visible slightly offset from the apex of the wider front end (Fig. 2*F*, left-hand bright-field image). It is the accentuation of this during the constriction of invasion depicted within

classic electron microscopy images which has likely led to the general assumption that merozoites uniformly narrow toward the apical end (Fig. 2*F*). While this is most clearly seen in the elongated forms of the *P. knowlesi* merozoites, it is also demonstrated in videos of gliding in *P. falciparum* (Movie S2).

Merozoites also exhibited helical motility during host cell entry and after internalization within the host cell, as has been described for invading *T. gondii* tachyzoites (12). This event can be seen when observing apically localized AMA1-mNG, which rotates around the plane of the moving junction in an anticlockwise manner during entry and then again rapidly for several seconds postinternalization (Movie S6). Thus, like other zoites, *Plasmodium* merozoites appear to enter host cells using a

Yahata et al.
Gliding motility of *Plasmodium* merozoites

PNAS | 3 of 10
https://doi.org/10.1073/pnas.2114442118

MICROBIOLOGY

corkscrew-like mechanism. Post entry spinning, as recently visualized with 4D lattice light sheet microscopy for invading *P. falciparum* parasites (28), may, in turn, facilitate twisting and separation of the newly formed parasitophorous vacuole from the erythrocyte plasma membrane.

**Gliding Motility Is Powered by an Actomyosin Motor and Glideosome Complex.** To determine the characteristics of the *P. falciparum* merozoite glideosome, we evaluated the effect of chemical compounds and parasite genetic modifications on merozoite gliding motility. In comparison to *P. knowlesi*, *P. falciparum* merozoites appear to be more vulnerable to light (29) and often lose their ability to invade erythrocytes when exposed to even small amounts of light, complicating the observation of their gliding movement by light microscopy. In our hands, schizonts exposed to light over several minutes often showed very few motile merozoites (Movie S7). On average, only roughly 6% (2/32) of schizonts released 70% or more gliding merozoites, where a "glide" was defined as forward movement for at least five continuous seconds (*SI Appendix*, Fig. S3*A* and Movie S2). Thus, to overcome the light sensitivity of *P. falciparum* merozoites, we developed an assay in which schizonts were seeded and incubated in the dark on coverslips for 1 h at 37 °C until the completion of merozoite egress. Motility could then be quantified by measuring the distance between a DAPI-stained merozoite nucleus and the hemozoin in the residual body (Fig. 3A). In comparing with dimethyl sulfoxide (DMSO)-treated merozoites (100%), 0.1, 1, and 10 μM cytochalasin ($IC_{50}$ = 0.085 μM) D treatment significantly reduced the merozoite–hemozoin distance (77.9%, IQR = 25.1%; 52.6%, IQR = 28.2%; and 50.9%, IQR = 16.5%, respectively). Treatment with jasplakinolide, an actin filament stabilizer reported to increase the speed of *T. gondii* tachyzoites, did not significantly increase the distance traveled by *P. falciparum* merozoites (Fig. 3B and *SI Appendix*, Fig. S3*B*).

We next examined the effects of the conditional deletion of two essential glideosome components, ACT1 (16) and GAP45 (17). Transgenic lines were able to egress both after the control DMSO treatment and upon rapamycin-induced gene excision, but the merozoite–hemozoin distance was significantly reduced after deletion of either ACT1 or GAP45 (Fig. 3C). When AMA1, a microneme protein important for erythrocyte invasion but unlikely to be involved in merozoite motility (30, 31), was conditionally deleted, parasites were able to efficiently egress and move across the substrate (*SI Appendix*, Fig. S4). These results confirm the requirement of the glideosome for *Plasmodium* merozoite gliding motility.

**Gliding Motility Is Regulated by a Complex Signaling Pathway.** Microneme discharge plays an essential role in the egress, gliding motility, and cell invasion of apicomplexan parasites and is regulated by a set of intracellular signaling enzymes, including calcium-dependent protein kinases (32, 33), phosphoinositide phospholipase C (PI-PLC) (34), and diacylglycerol (DAG) kinase (35). We evaluated whether these enzymes are also involved in the gliding motility of *P. falciparum* merozoites. Although the calcium ionophore A23187 (up to 100 μM) did not show a significant effect, the calcium chelator BAPTA-AM (10 μM) significantly reduced merozoite–hemozoin distance ($P < 0.0001$; Fig. 3D and *SI Appendix*, Fig. S3*B*). The PLC inhibitor U73122 (1 μM), but not the inactive analog U73343 (up to 10 μM), significantly reduced merozoite–hemozoin distance ($P < 0.0001$). The DAG kinase inhibitor R59022 (3 μM), which inhibits the conversion of DAG to phosphatidic acid (PA), also significantly reduced movement ($P < 0.001$), while the merozoite–hemozoin distance was not changed with propranolol, an inhibitor of phosphatidate phosphohydrolase (the converter of PA to DAG). Collectively, these results are consistent with reports on *Toxoplasma* tachyzoites (35) and indicate that complex signaling pathways are involved in gliding motility of *P. falciparum* merozoites (Fig. 3E).

**Gliding Motility Facilitates Erythrocyte-Specific Interactions and Underpins Important Precursor Steps to Invasion.** Having established the characteristics of merozoite motility and its regulation, we next sought to understand whether gliding may play a role during erythrocyte invasion in addition to host cell entry, and whether this function might also facilitate movement of merozoites across alternative cellular surfaces. Prior to host cell entry, merozoite–erythrocyte interactions cause the erythrocyte membrane to deform, often resulting in the entire erythrocyte "wrapping" around the merozoite (7). Several studies have highlighted the importance of deformation as a mechanism merozoites use to commit to host cell entry and have demonstrated that the merozoite's molecular motor is required for deformation (16, 17, 36). However, the precise mechanism behind this phenomenon has not been elucidated. In good agreement with previous work, we found that, not only were rapamycin-treated ACT1- or GAP45-deleted *P. falciparum* parasites unable to glide, but they were also unable to deform erythrocytes (Fig. 4 *A* and *B*). Thus, we reasoned that gliding motility itself may be required for erythrocyte deformation.

Due to our finding that the majority of *P. knowlesi* merozoites do not disperse from each other when gliding is inhibited with cytochalasin D, we could not easily measure the impact of gliding inhibition on erythrocyte deformation for this species. However, the larger size and more pronounced morphology of *P. knowlesi* merozoites did allow us to visualize the deformation process of wild-type merozoites more clearly. Deformation did not appear to simply be the result of the merozoite attempting to be internalized in the erythrocyte, as previously hypothesized (6). Rather, deformation was marked by a wrapping of the erythrocyte membrane down the length of a forward-moving merozoite, horizontally aligned with the erythrocyte surface. Notably, deformation began as a merozoite initiated gliding across a host cell surface, with waves of deformation often traveling from the zoite's apical prominence to the basal end (Fig. 4*C* and Movie S8). These sum results indicate that, not only does gliding motility coincide with erythrocyte deformation, but also the two processes are mechanically linked.

Recently, both sexual and asexual stages of multiple *Plasmodium* species have been identified within bone marrow compartments (37–39). This raised the question of whether merozoites may be able to glide on endothelial surfaces and/or within extravascular compartments, such as the bone marrow. Yet how do *Plasmodium* parasites exit the bloodstream and enter tissues? One possibility is that parasitized reticulocytes may be returning to extravascular environments via extravasation. However, another mechanism could be that free merozoites are capable of gliding across endothelial barriers and into tissues (40, 41). To test the latter theory, we examined *P. knowlesi* parasites egressing on either primary human umbilical vein endothelial cells (HUVECs) or dermal endothelial cell lines. Rather surprisingly, we found that *P. knowlesi* merozoites were unable to adhere to or demonstrate motility across either cell line (Fig. 4*D* and Movie S9). Similar results were obtained when endothelial cells were pretreated with tumor necrosis factor (TNF), an inflammatory cytokine known to increase the expression of endothelial adhesive surface ligands (Fig. 4*D*) (42). Thus, while these results do not rule out the possibility of gliding within tissue compartments, they do suggest that gliding is unlikely to support extravasation of free merozoites and that merozoite motility may be specific to erythrocyte lineages and highly adherent artificial surfaces. While sporozoites are known to glide readily in both mosquito and human tissue environments, they have recently been shown to not glide on HUVECs
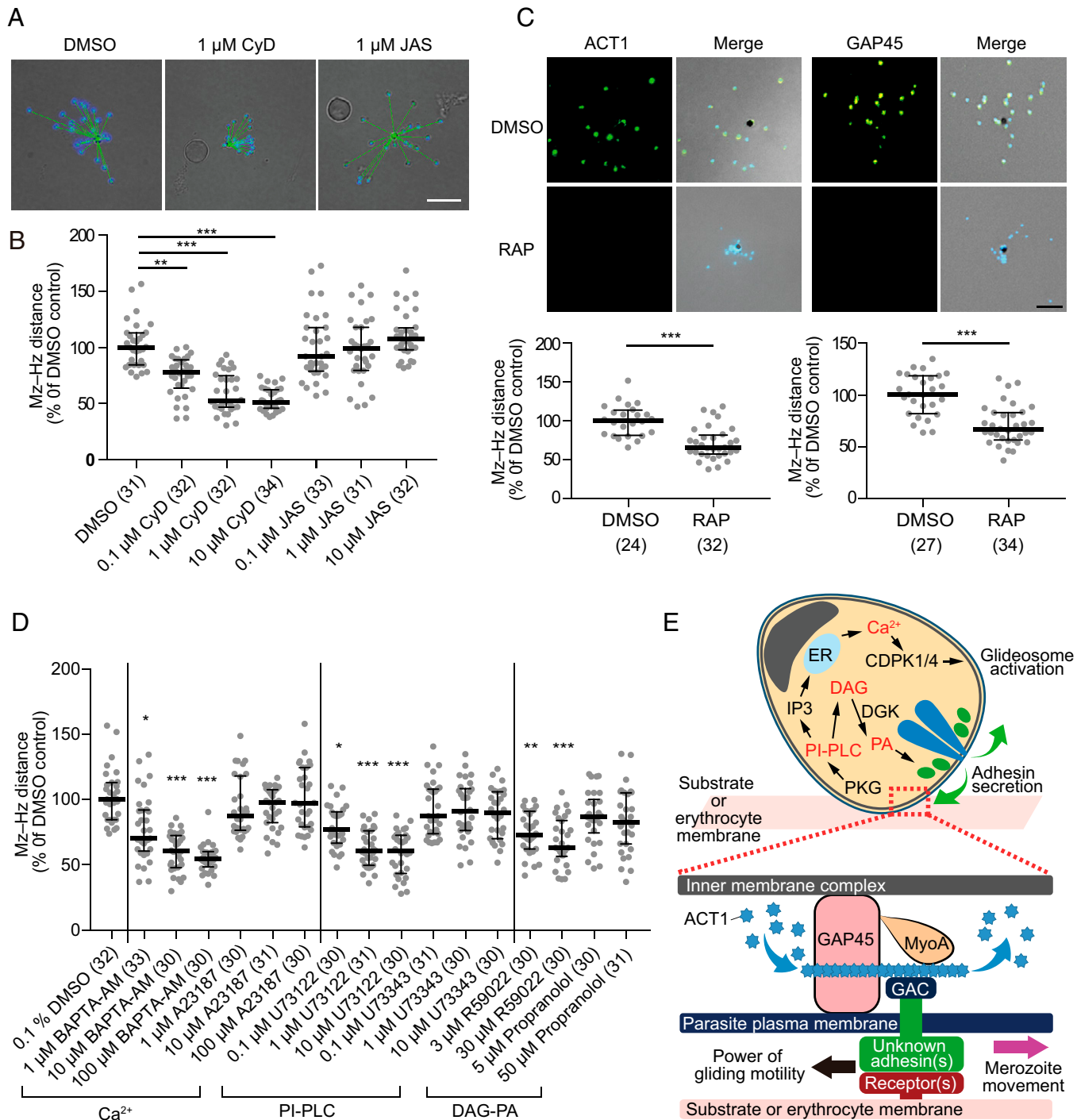
**Fig. 3.** The effects of chemical compounds and parasite genetic modifications on *P. falciparum* merozoite gliding motility. Purified *P. falciparum* schizonts were seeded on the coverslip, and merozoites were left to egress for 1 h. (*A*) The distance of the merozoite (Mz) nucleus (DAPI) from hemozoin (Hz) (black pigment) was measured (green line, Mz–Hz distance). (*B* and *C*) Where indicated in the *y* axes, the relative Mz–Hz distances compared to DMSO control obtained from each schizont with their median and interquartile range are shown. The number of analyzed schizonts from three independent experiments is indicated in parentheses. (Scale bar, 5 μm.) (*B*) Effects of 0.1% DMSO, 0.1, 1, or 10 μM cytochalasin D (CyD, IC$_{50}$ = 0.085 ± 0.029 μM), or jasplakinolide (JAS, IC$_{50}$ = 0.110 ± 0.019 μM) were evaluated for merozoite gliding motility; ** and *** indicate $P < 0.001$, and $< 0.0001$, respectively. (*C*) Inhibition of gliding motility in rapamycin (RAP)-treated ACT1- or GAP45-deleted *P. falciparum* parasites. The indirect immunofluorescence assay with specific antibodies indicated ACT1 or GAP45 were not detected in RAP-treated transgenic parasites; *** indicates $P < 0.0001$ by the Mann–Whitney test. (Scale bar, 5 μm.) (*D*) Purified *P. falciparum* schizonts were treated with BAPTA-AM (IC$_{50}$ = 0.992 ± 0.187 μM), A23187 (IC$_{50}$ = 0.588 ± 0.029 μM), U73122 (IC$_{50}$ = 0.271 ± 0.085 μM), U73343 (IC$_{50}$ = 5.444 ± 0.199 μM), R59022 (IC$_{50}$ = 4.678 ± 0.392 μM), or propranolol (IC$_{50}$ = 0.551 ± 0.135 μM), and merozoite gliding assays were performed. The relative Mz–Hz distances compared to DMSO control obtained from each schizont with their median and interquartile range are shown. The number of analyzed schizonts from three independent experiments is indicated in parentheses; *, **, and *** indicate $P < 0.05$, $< 0.001$, and $< 0.0001$, respectively. (*E*) Overview of molecular mechanisms for gliding motility of *P. falciparum* merozoite. After merozoite egress from the erythrocyte, merozoite adhesin(s) are secreted from micronemes (green) via a signaling pathway involving PI-PLC and DAG kinase (DGK) and bind to environmental substrates including the erythrocyte membrane. A pathway involving PI-PLC and Ca$^{2+}$ activates calcium-dependent protein kinases (CDPKs) and phosphorylates the components of the glideosome machinery (32–35, 64). Gray, nucleus; blue, rhoptries. Gliding motility is powered by an actomyosin motor of the glideosome machinery, and the merozoite movement is transferred to the erythrocyte membrane, causing erythrocyte deformation upon merozoite attachment. ACT1, actin-1; PKG, cyclic GMP-dependent protein kinase; GAP45, glideosome-associated protein 45; MyoA, myosin-A; and GAC, glideosome-associated connector.

(18)—suggesting that specific cell types may be nonpermissive for motility even for zoites with relatively broad gliding substrate specificities.

Despite the finding that merozoites are unlikely to use gliding to move across endothelial barriers, we did observe that freshly egressed *P. knowlesi* merozoites often glide across several different human erythrocytes prior to invading their host cell of choice (Movie S10). Thus, we reasoned that, in addition to facilitating erythrocyte deformation, gliding may enable

merozoites to contact multiple erythrocytes, in the event they are unable to invade the first host cell they encounter. Studies have shown that most invading *P. falciparum* merozoites (~85%) will invade the first cell they contact (36); however, we found that only 26% (10/38 invasions) of invading *P. knowlesi* merozoites invaded the first human erythrocyte they contacted, and a significant proportion of merozoites (~32%, or 12/38 events) contacted four to seven unique cells prior to committing to invasion (Fig. 4*E*). We hypothesized that this stark
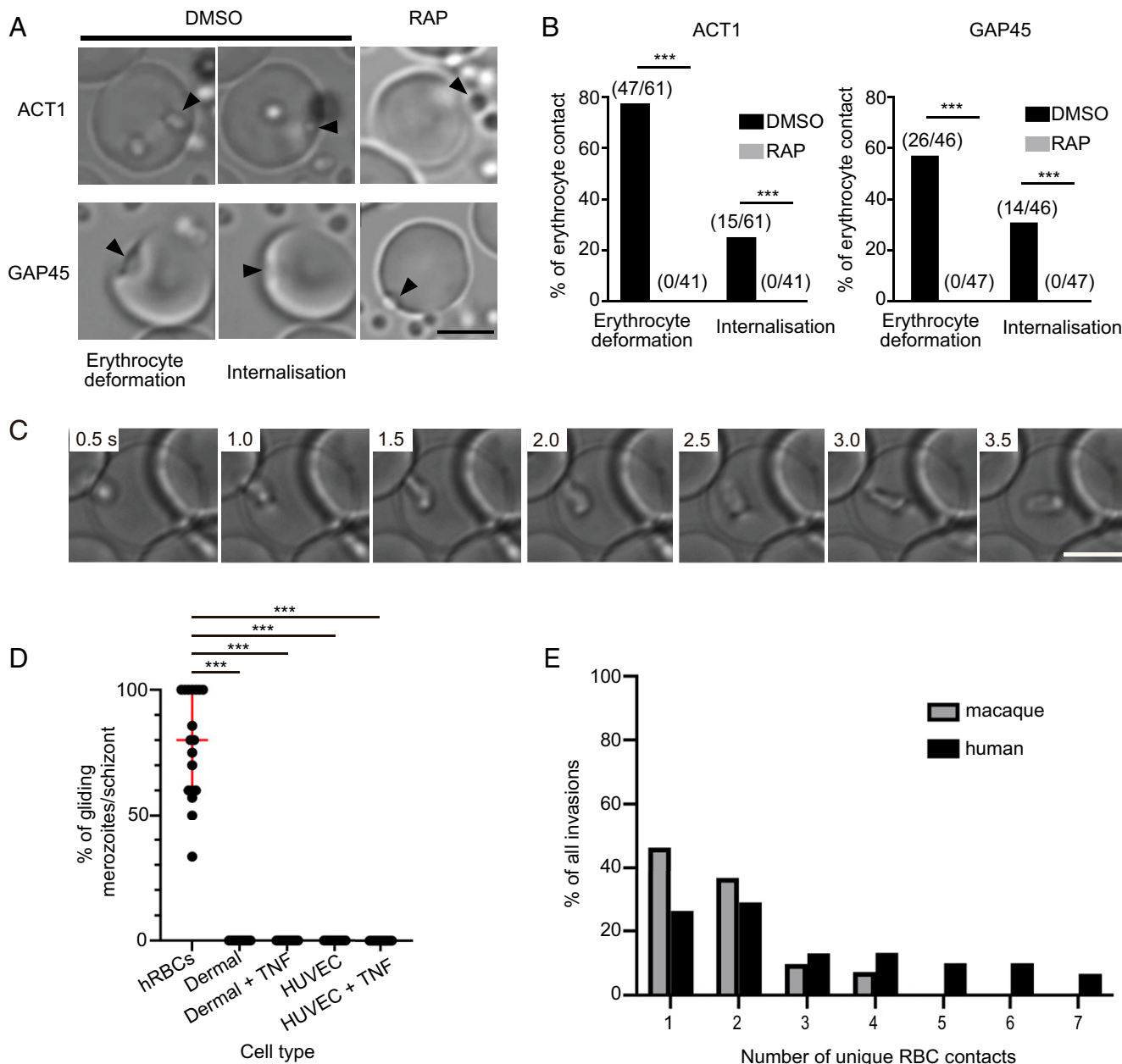


**Fig. 4.** A role for gliding motility in facilitating merozoite–erythrocyte interactions. (*A* and *B*) Erythrocyte deformation and merozoite internalization events were seen for DMSO-treated ACT1- or GAP45-floxed *P. falciparum* parasites, but not detected after RAP treatment (***$P < 0.001$ by two-tailed Fisher's exact test). Arrowhead indicates a merozoite. (Scale bar, 5 μm.) (*C*) Still images taken from Movie S7, depicting a *P. knowlesi* merozoite beginning to deform a human erythrocyte as gliding motility is initiated along the surface of the host cell. (Scale bar, 5 μm.) (*D*) A median 80% of merozoites within a given schizont demonstrate gliding motility along human erythrocytes (*n* = 18 schizonts). In contrast, no gliding is observed at all on either TNF stimulated or nonstimulated HUVECs (*n* = 16 and 10 schizonts, respectively) and dermal endothelial cells (*n* = 16 and 10 schizonts, respectively). Comparisons were made by one-way ANOVA, using a Kruskal–Wallis test; ***$P < 0.0001$. (*E*) The total number of unique erythrocyte contacts each invading merozoite made was significantly lower for macaque (*n* = 41 invasions) vs. human (*n* = 38 invasions) erythrocyte invasions. Comparisons were made using Poisson regression (Poisson coefficient 0.076, 95% CI: 0.37 to 0.52; $P < 0.001$).

difference between species may be because, unlike *P. falciparum*, the natural host cells of *P. knowlesi* are not human, but rather are macaque erythrocytes (23). Thus *P. knowlesi* merozoites may need to contact more human erythrocytes overall to encounter an erythrocyte amenable to invasion. In support of this theory, we found that, on average, *P. knowlesi* merozoites contacted significantly fewer macaque erythrocytes prior to invasion (Fig. 4*E*), with the vast majority of merozoites (85%) invading either the first or second macaque cell they contacted. Therefore, these results indicate that gliding could contribute to the zoonotic potential of *P. knowlesi* and may explain how merozoites of multiple species navigate strict erythrocyte tropism requirements to proliferate under suboptimal conditions.

## Discussion

In this work, we show that *Plasmodium* merozoites undergo gliding motility and demonstrate productive movement across coverslip and erythrocyte surfaces for two human infective species: *P. falciparum* and *P. knowlesi*. Motility was more evident for *P. knowlesi* merozoites, which, in our hands, were found to glide, on average, nearly twice as fast and for 7 times longer than *P. falciparum* merozoites.

Since the first, and landmark, video microscopy of *P. knowlesi* in 1975 (6), no further imaging studies have been published for this species. This, in combination with the frequent use of glass slides to image parasites, rather than the polymer coverslips that were used for this study, may explain, in part, why motility was not observed in *P. falciparum* invasion studies. However, our retrospective analysis of published data shows several subtle examples of *P. falciparum* merozoites completing short glides across human erythrocytes, such as videos from Treeck et al. (ref. 30, video S4, from 25 s to 70 s) and Weiss et al. (ref. 36, video S13, from 0 s to 26 s) (36).

Our work, in good agreement with previous studies (16, 17, 36), shows that, without motor function, merozoites cannot glide across cellular surfaces or deform host erythrocytes. Thus, gliding motility is likely an important requirement for deformation. While deformation itself is not an essential invasion step for *P. falciparum*, strong deformation has been positively correlated with invasion success and is predicted to increase the efficiency of the host cell selection process (36). Therefore, by extension, gliding is also likely to facilitate these key steps, increasing the likelihood of each merozoite–erythrocyte contact progressing into invasion.

Having clearly demonstrated gliding motility in static in vitro cultures, it will be important to determine how this mechanism translates to flow conditions found in vivo. While the feasibility of cell–cell transfer is yet to be tested under flow conditions, live in vivo imaging of erythrocytes flowing through human capillaries shows that erythrocytes are frequently attached to each other for prolonged periods of time, traveling together at roughly the same speed (43). Therefore, in theory, flowing erythrocyte "bridges" may facilitate merozoite movement from cell to cell in vivo.

Erythrocytes are known to be highly heterogeneous, in terms of maturity, surface receptor density, and membrane tension properties (44). As such, motility could also enable merozoites to contact a wider range of erythrocytes in the bloodstream, whereby the parasite moves around the surface of an individual erythrocyte or across the surfaces of multiple erythrocytes until it is able to engage with a critical threshold of invasion receptors or select a cell with favorable characteristics for invasion. Our work has shown that only 26% of *P. knowlesi* merozoites invade the first human erythrocyte they contact, with the vast majority instead contacting multiple cells before committing to invasion. Notably, *P. knowlesi* exhibits a preference (not restriction) for younger erythrocytes when cultured with human

erythrocytes (45, 46). Thus, gliding may be a critical mechanism *P. knowlesi* merozoites use to successfully proliferate in human hosts.

A greater proportion of *P. knowlesi* merozoites will invade the first macaque erythrocyte they contact (∼46%), in line with their preference for their natural host cells (macaque erythrocytes) over human cells (45). In contrast, most *P. falciparum* merozoites (∼86% of 3D7 parasites) invade the first human erythrocyte they encounter (36); therefore, the ability to contact multiple cells is likely to be less important for *P. falciparum*, and, instead, gliding may simply enhance erythrocyte receptor interactions on any given cell.

One reason for these distinct strategies could be that each species possesses highly divergent sets of RBL/Rh and DBP/EBA ligands—two critical families of invasion ligands which are key determinants of host cell tropism and are predicted to facilitate host cell selection (36, 47). Differing expression profiles, along with differing levels of receptor abundance and availability within erythrocyte populations, likely impact how efficiently merozoites can "commit" to invasion, and thus their need to contact different cells. At one extreme, for *Plasmodium vivax*, a single DBP ligand and selection of RBL ligands restricts this species to growth in Duffy positive human reticulocytes (48, 49). Since reticulocytes make up less than 2% of red blood cells circulating within the bloodstream (50), gliding motility may enable *P. vivax* merozoites to roam and eventually encounter reticulocytes.

It is also plausible that motility supports translocation and invasion within tissues such as the bone marrow, which is known to be a significant parasite reservoir for *P. vivax* (39). Parasites may accumulate within the bone marrow via extravasation: the crossing of either infected reticulocytes or free merozoites into the bone marrow parenchyma via a layer of endothelial cells lining the sinusoidal capillaries (40, 41). However, we did not observe merozoite motility across endothelial surfaces, an outcome which suggests that gliding may not support extravasation of free merozoites. Work examining how ookinetes and sporozoites glide through different environments has identified key differences in gliding behavior on varying cell types and substrate elasticity. Sporozoites were shown to be unable to glide on HUVECs, with evidence suggesting this was, in part, due to sporozoites gliding poorly on the relatively soft substrate provided by this cell type (18). The role of this adaptation was suggested that ensure sporozoites, once inside the bloodstream, quickly flow to the liver sinusoids, and do not exit the blood stream prematurely. Similarly, for merozoites, the adaptation ensures that they do not adhere to or glide across cells nonpermissive for invasion.

Notably, however, *P. vivax* merozoites have been shown to exhibit a preference for the CD71-positive youngest reticulocytes found predominantly within the bone marrow prior to further maturation and intravasation (40). This suggests that at least some invasions may take place within the bone marrow parenchyma itself, contributing to the overall parasite burden within this tissue. Thus, gliding may enable merozoites that have egressed within the bone marrow to specifically target these young reticulocytes in this richly diverse cellular environment.

Our work also enabled us to reverse the perception of the morphology of merozoites, with clear evidence from both gliding and fluorescently tagged parasites demonstrating that the apical complex resides in a small protrusion in the wider end of the zoite, rather than in the pointed end of a teardrop shape as is often depicted (51). *Plasmodium* ookinetes also lead with their wider end (19), and thus how we interpret images of invasion and understand the biophysical processes involved must be reevaluated (51).

Our displacement assay also enabled us to test the impact of various inhibitors of calcium signaling pathways, previously

Yahata et al.
Gliding motility of *Plasmodium* merozoites

PNAS | 7 of 10
https://doi.org/10.1073/pnas.2114442118

shown to be important for microneme secretion (34) and invasion (34, 36) for *Plasmodium* parasites. Our results are in good agreement with data from these studies; however, ascribing function based on inhibitor data alone can be challenging. For instance, although our work shows that the inhibitor U73122, but not its inactive analog, U73343, inhibits signaling pathways also predicted to be required for motility; in other systems, the effects of both compounds have been shown to be identical, suggesting off-target activity (52). Therefore, future work should include targeted genetic approaches such as conditional knockout studies ablating signaling enzymes—something which is now readily achievable for *Plasmodium* blood stages in both *P. knowlesi* and *P. falciparum* (53).

One of the outstanding questions is which parasite proteins are required for bridging the motor to host cell ligands to enable gliding motility. Apicomplexan zoites utilize type I transmembrane proteins belonging to the TRAP family to adhere to environmental substrates for gliding. Two such proteins, merozoite thrombospondin-related anonymous protein (MTRAP) and thrombospondin-related apical membrane protein (TRAMP or PTRAMP), are expressed at the merozoite stage (54). MTRAP is dispensable for *P. falciparum* and *P. berghei* merozoites (55); however, multiple studies indicate that TRAMP is essential for the blood-stage parasite (56, 57), making it a prime candidate for future work to identify a merozoite gliding adhesin. Our gliding assays can greatly facilitate the identification of such proteins and their roles during invasion.

In conclusion, *Plasmodium* merozoites have the capacity for gliding motility, powered by a conserved actomyosin motor and glideosome complex, and controlled by a complex signaling cascade. The distinct gliding profiles of two different human infective species suggest divergent invasion strategies which provide new mechanisms to address questions of host selectivity and tissue reservoirs of the erythrocytic stages.

## Materials and Methods

**Parasite Culture and Transfection.** *P. falciparum* Dd2 parasites were maintained with deidentified O⁺ human erythrocytes (Japanese Red Cross Blood Society) in Roswell Park Memorial Institute (RPMI) 1640 medium (Invitrogen) supplemented with 25 mM Hepes (Sigma), 0.225% sodium bicarbonate (Invitrogen), 0.1 mM hypoxanthine (Sigma), 25 μg/mL gentamicin (Invitrogen), and 0.5% AlbuMax I (Invitrogen), essentially as described (58). The ACT1 (16), GAP45:loxP (17), and AMA1:loxP *P. falciparum* lines (59) were cultured with A⁺ human erythrocytes. WR99210 and G418 were used to generate ACT1 and AMA1:loxP parasite lines, respectively. *P. yoelii* 17XNL parasites were intravenously inoculated into Institute of Cancer Research mice (SLC Inc.). Animal experiments were approved by the Animal Care and Use Committee of Nagasaki University (Permit 1403031120-5). The *T. gondii* RH strain was cultured in a confluent monolayer of human foreskin fibroblasts (HFFs) maintained in Dulbecco's Modified Eagle Medium (DMEM) and GlutaMAX supplemented with 10% fetal bovine serum, at 37 °C and 5% CO₂. The *B. bovis* Texas strain was maintained in purified bovine erythrocytes with GIT medium (WAKO) at 37 °C with a microaerophilic stationary-phase culture system. A1-H.1 *P. knowlesi* parasites were maintained in deidentified human erythrocytes (UK National Blood Transfusion Service) with custom-made RPMI-1640 medium, supplemented with 10% horse serum (vol/vol) and 2 mM L-glutamine according to previously described methods (23). Mature schizonts were purified by gradient centrifugation on a 55% Nycodenz layer (Progen), as described (23). Tightly synchronized schizonts were transfected using the Amaxa 4-D electroporator and P3 Primary Cell 4D Nucleofector X Kit L (Lonza) according to the protocol described by Moon et al. (23).

**Generation of *P. knowlesi* Parasites with mNeonGreen-Tagged AMA1.** *P. knowlesi* parasites with mNeonGreen-tagged AMA1 were generated by insertion of an mNeonGreen sequence immediately before the *AMA1* stop codon (*SI Appendix*, Fig. S2A) using the CRISPR-Cas9 system described by Mohring et al. (60) (single guide RNA sequence: GAGAAGCCTTACTACTGAGT). Donor DNA was synthesized by overlapping PCR, as previously described for PkAMA1-HA tagged parasites (60), and included the mNeonGreen sequence flanked by 500-bp sequences homologous to the C-terminal (HR1) and 3′UTR (HR2) regions of the AMA1 locus (*SI Appendix*, Fig. S2A). Primers for PCR and

DNA fragments are listed in *SI Appendix*, Table S1 and Table S2. In brief, HR1 and HR2 were both PCR amplified from *P. knowlesi* A1-H.1 genomic DNA (with primers P6/P7 and P8/P9, respectively), while the mNeonGreen sequence was amplified from plasmid Pk_mNeonGreen with primers P10/P11. All three fragments were subsequently assembled together in two successive steps: firstly, by fusing fragments HR1 and mNeonGreen (primers P12/P13), and, secondly, by fusing fragments HR1/mNeonGreen and HR2 (primers P12/P15) to create the final product, HR1/mNeonGreen/HR2. Post transfection, integration of donor DNA was confirmed by diagnostic PCR, using primers P1 and P3 (*SI Appendix*, Fig. S2B). Expression of the AMA1-mNeonGreen fusion protein was also confirmed by indirect immunofluorescence assay (*SI Appendix*, Fig. S2C). Air-dried smears of late-stage schizonts were fixed in 4% paraformaldehyde for half an hour and permeabilized with phosphate-buffered saline (PBS) containing 0.1% Triton-X100 for 10 min. Slides were subsequently blocked overnight in PBS containing 3% BSA before labeling with anti-mNeonGreen mouse monoclonal antibody (32F6; 1:300; Chromotek) followed by Alexa Fluor 488 goat anti-mouse antibody (1:1,000, Invitrogen). Nuclei were stained with DAPI (Invitrogen) and mounted with ProLong Gold antifade reagent (Invitrogen). Images were collected using an inverted microscope (Ti-E; Nikon) with a 60× oil objective lens (N.A. 1.4).

**Inducible Gene Knockout *P. falciparum* Parasites.** The *GAP45*, *Act1*, and *AMA1* genes were excised by rapamycin treatment from GAP45:loxP, ACT1, and AMA1:loxP *P. falciparum* parasites, respectively (61). Briefly, ring-stage parasites synchronized by 5% sorbitol method were treated with 100 nM rapamycin (Sigma) or 0.1% DMSO for 12 h. Schizonts were purified with a CS magnet separation column (MACS, Miltenyi Biotech) and used for gliding or erythrocyte invasion assays.

**Endothelial Cell Culture and Stimulation** Commercially available primary human dermal microvascular endothelial cells (HDMVECs, ScienCell) and HUVECs (ScienCell) were cultured at 37 °C with 5% CO₂ on fibronectin-coated six-channel μ-Slides (ibidi) and grown to confluence in DME/F12 medium (Thermo Fisher), pH 7.4, supplemented with 10% fetal bovine serum (ScienCell), 30 μg/mL endothelial cell growth supplement (Sigma), and 10 μg/mL gentamicin (Thermo Fisher). Cells were rinsed with sterile PBS (Sigma), and fresh medium was added 18 h prior to the gliding assays, with or without 10 pg/mL recombinant human TNF alpha (TNFα, PeproTech). Primary HDMVECs and HUVECs were used between passages 2 and 3 for all experiments.

**Time-Lapse Imaging for the Gliding Motility.** Time-lapse imaging assays for *P. falciparum* merozoites were performed at 37 °C using an inverted microscope (Ti-E; Nikon) with a 60× oil objective lens (N.A. 1.4 or 1.47). *P. falciparum* synchronized schizonts in incomplete medium without AlbuMAX I were transferred to the ibiTreat μ-Slide I⁰·⁴ Luer channel slide (ibidi) and incubated for 10 min at 37 °C to allow the parasite-infected erythrocytes to attach to the bottom. Incomplete medium was removed and replaced with complete RPMI medium prewarmed to 37 °C; then parasites were observed by microscopy. Likewise, synchronized *P. knowlesi* schizonts were transferred, using the same technique, to either ibiTreat, poly-L-lysine–coated, uncoated, or glass μ-Slide I⁰·⁴/⁰·⁵ Luer channel slides (ibidi) in incomplete RPMI medium and incubated at 37 °C for 10 min to allow cell attachment. Subsequently, incomplete medium was replaced with complete RPMI medium with 10% horse serum, as per normal culturing conditions. For the actin inhibitor treatments, *P. knowlesi* schizonts were allowed to attach to coverslips while suspended in incomplete RPMI medium, which was then replaced with complete RPMI medium additionally containing 0.1 μM cytochalasin D (Sigma) or 0.1% DMSO (Sigma). For experiments visualizing *P. knowlesi* egress, schizonts were first incubated with 10 μg/mL wheat germ agglutinin for 10 min at 37 °C. Schizonts were subsequently washed two times in RPMI medium before loading into channel slides for drug treatment as described above. For *P. knowlesi* invasion assays, purified schizonts were added to fresh human (UK National Blood Transfusion Service) or cynomolgus macaque (Silabe) erythrocytes to make a 5 to 10% parasitaemia and 2.5% hematocrit culture. The hematocrit was subsequently adjusted to 0.25%, and 150 μL of culture was loaded into a PLL-coated μ-Slide VI 0.4 (ibidi). *P. yoelii* sporozoites were isolated in RPMI medium from parasite-infected mosquito midguts as described (62); then isolated sporozoites were transferred to an ibiTreat μ-Slide I⁰·⁴ Luer channel slide. *T. gondii* tachyzoites growing in HFFs were collected by scraping after the culture medium was replaced with Endo buffer (63). Intracellular parasites were isolated from HFFs by lysing host cells via passaging 20 times through a syringe, and tachyzoites were transferred to an ibiTreat μ-Slide I⁰·⁴ Luer channel slide and incubated for 15 min at 37 °C. The slide was placed on the microscope stage, and the medium was replaced with DMEM before observation. *B. bovis* parasites were isolated in RPMI medium, and then transferred to the ibiTreat

µ-Slide I⁰·⁴ Luer channel slide. All parasites were observed by differential interference contrast or bright field at 1.5 V/100 W of halogen lamp or LED light (pT-100; CoolLED) to minimize cell damage. Time-lapse images were captured at 1 to 100 frames per second using a digital camera (ORCA-R2 or ORCA-Flash4.0; Hamamatsu Photonics) and imaged using NIS-Element Advanced Research imaging software (Nikon). The speed of individual merozoites was calculated by tracking actively moving merozoites manually, using distance measurement tools, or by the tracking module within the NIS-Element software (Nikon). The tangential speed of *P. knowlesi* merozoites was determined by calculating the number of rotations per minute and multiplying this value by the average circumference of a merozoite. The angle of the motor was subsequently calculated using the formula $\tan(x) = R/L$, where $x$ = the angle of the motor, $R$ = the average distance each merozoite rotated/per body length traveled forward, and $L$ = the body length of the merozoite.

**P. falciparum Merozoite Gliding Assay.** *P. falciparum* schizonts were purified with a CS magnet separation column, then adjusted to $1 \times 10^5$ cells per mL with incomplete RPMI medium and loaded onto an ibiTreat µ-Slide VI⁰·⁴ channel slide (ibidi). The channel slides were incubated for 10 min at 17 °C to allow schizont attachment to the bottom, followed by replacing the medium with complete RPMI medium containing chemical compounds or DMSO control. Slides were incubated at 17 °C for 1 h, and then the temperature was increased to 37 °C for 1 h to allow parasite egress. Parasites were fixed with 1% paraformaldehyde fixation solution, which was then replaced with PBS containing 3% BSA (Sigma) and 100 ng/mL DAPI. For the indirect immunofluorescence assay, parasites were fixed in 4% paraformaldehyde containing 0.0075% glutaraldehyde (Nacalai Tesque) and permeabilized with PBS containing 0.1% Triton-X100 (Calbiochem), and then blocked with PBS containing 3% BSA. Next, samples were immunostained with mouse anti-*P. falciparum* ACT1 (final dilution 1:500; a kind gift from Jake Baum, Department of Life Sciences, Imperial College London, UK) or rat anti-HA (1:1,000; Roche) for HA-tagged GAP45 and AMA1. This was followed by 3× washes with PBS and then incubation with Alexa Fluor 488 goat anti-mouse or Alexa Fluor 594 goat anti-rat antibodies (1:1,000; Invitrogen) in PBS containing 3% BSA with DAPI. Stained parasites were mounted with Prolong Gold antifade reagent. Microscopy images (Ti-E, Nikon) of egressed merozoites were cropped to $47 \times 47$ µm$^2$ to measure the distance of merozoite nuclei (stained with DAPI) from hemozoin in the residual body (malaria pigment, with bright-field image) using NIS-Elements software (Nikon). Statistical analysis was performed by the Kruskal–Wallis test followed by Dunn's multiple comparison test using PRISM 6 software (GraphPad Software, Inc.).

**Chemical Compounds.** Complete RPMI medium was supplemented with cytochalasin D, jasplakinolide (Sigma), 1,2-Bis(2-aminophenoxy)ethane-N,N,N′,N′-tetraacetic acid tetraacetoxymethyl ester (BAPTA-AM, Invitrogen), calcium Ionophore A23187 (Sigma), U73122 (Calbiochem), U73343 (Calbiochem), R59022 (Tocris Bioscience), propranolol (Sigma), or DMSO. Compound concentrations were as described (33, 34). IC$_{50}$ values for *P. falciparum* were determined using a protocol available at WorldWide Antimalarial Resistance Network (https://www.wwarn.org/sites/default/files/INV08_PFalciparumDrug-Sensitivity.pdf).

**Data Availability.** All study data are included in the article and/or supporting information.

1. D. G. Russell, R. E. Sinden, The role of the cytoskeleton in the motility of coccidian sporozoites. *J. Cell Sci.* **50**, 345–359 (1981).
2. J. M. Dobrowolski, L. D. Sibley, Toxoplasma invasion of mammalian cells is powered by the actin cytoskeleton of the parasite. *Cell* **84**, 933–939 (1996).
3. B. Danilewsky, *La Parasitologie Comparée du Sang* (Kharkoff, 1889).
4. B. Grassi, *Studi di Uno Zoologo Sulla Malaria* (Roma Accademia dei Lincei, 1900).
5. M. Yoeli, Movement of the sporozoites of Plasmodium berghei (Vincke et Lips, 1948). Nat*ure* **201**, 1344–1345 (1964).
6. J. A. Dvorak, L. H. Miller, W. C. Whitehouse, T. Shiroishi, Invasion of erythrocytes by malaria merozoites. *Science* **187**, 748–750 (1975).
7. P. R. Gilson, B. S. Crabb, Morphology and kinetics of the three distinct phases of red blood cell invasion by *Plasmodium falciparum* merozoites. *Int. J. Parasitol.* **39**, 91–96 (2009).
8. K. Yahata, M. Treeck, R. Culleton, T. W. Gilberger, O. Kaneko, Time-lapse imaging of red blood cell invasion by the rodent malaria parasite *Plasmodium yoelii. PLoS One* **7**, e50780 (2012).
9. I. Tardieux, J. Baum, Reassessing the mechanics of parasite motility and host-cell invasion. *J. Cell Biol.* **214**, 507–515 (2016).
10. S. Håkansson, H. Morisaki, J. Heuser, L. D. Sibley, Time-lapse video microscopy of gliding motility in *Toxoplasma gondii* reveals a novel, biphasic mechanism of cell locomotion. *Mol. Biol. Cell* **10**, 3539–3547 (1999).
11. K. Frénal, J. F. Dubremetz, M. Lebrun, D. Soldati-Favre, Gliding motility powers invasion and egress in Apicomplexa. *Nat. Rev. Microbiol.* **15**, 645–660 (2017).
12. G. Pavlou et al., *Toxoplasma* parasite twisting motion mechanically induces host cell membrane fission to complete invasion within a protective vacuole. *Cell Host Microbe* **24**, 81–96.e5 (2018).
13. C. Opitz, D. Soldati, 'The glideosome': A dynamic complex powering gliding motion and host cell invasion by *Toxoplasma gondii. Mol. Microbiol.* **45**, 597–604 (2002).
14. J. Baum et al., A conserved molecular motor drives cell invasion and gliding motility across malaria life cycle stages and other apicomplexan parasites. *J. Biol. Chem.* **281**, 5197–5208 (2006).
15. J. Robert-Paganin, et al., Plasmodium myosin A drives parasite invasion by an atypical force generating mechanism. *Nat. Commun.* **10**, 3286 (2019).
16. S. Das, L. Lemgruber, C. L. Tay, J. Baum, M. Meissner, Multiple essential functions of *Plasmodium falciparum* actin-1 during malaria blood-stage development. *BMC Biol.* **15**, 70 (2017).
17. A. J. Perrin et al., The actinomyosin motor drives malaria parasite red blood cell invasion but not egress. *MBio* **9**, e00905–e00918 (2018).
18. J. Ripp et al., Malaria parasites differentially sense environmental elasticity during transmission. *EMBO Mol. Med.* **13**, e13933 (2021).
19. R. W. Moon et al., A cyclic GMP signalling module that regulates gliding motility in a malaria parasite. *PLoS Pathog.* **5**, e1000599 (2009).
20. M. J. Boyle et al., Isolation of viable *Plasmodium falciparum* merozoites to define erythrocyte invasion events and advance vaccine and drug development. *Proc. Natl. Acad. Sci. U.S.A.* **107**, 14378–14383 (2010).
21. E. D. Dennis, G. H. Mitchell, G. A. Butcher, S. Cohen, In vitro isolation of *Plasmodium knowlesi* merozoites using polycarbonate sieves. *Parasitology* **71**, 475–481 (1975).
22. O. Lyth et al., Cellular dissection of malaria parasite invasion of human erythrocytes using viable *Plasmodium knowlesi* merozoites. *Sci. Rep.* **8**, 10165 (2018).
23. R. W. Moon et al., Adaptation of the genetically tractable malaria pathogen *Plasmodium knowlesi* to continuous culture in human erythrocytes. *Proc. Natl. Acad. Sci. U.S.A.* **110**, 531–536 (2013).
24. M. Kudryashev et al., Structural basis for chirality and directional motility of *Plasmodium* sporozoites. *Cell. Microbiol.* **14**, 1757–1768 (2012).
25. M. Asada et al., Gliding motility of *Babesia bovis* merozoites visualized by time-lapse video microscopy. *PLoS One* **7**, e35227 (2012).
26. A. Kan et al., Quantitative analysis of *Plasmodium* ookinete motion in three dimensions suggests a critical role for cell shape in the biomechanics of malaria parasite gliding motility. *Cell. Microbiol.* **16**, 734–750 (2014).
27. L. H. Miller, M. Aikawa, J. G. Johnson, T. Shiroishi, Interaction between cytochalasin B-treated malarial parasites and erythrocytes. Attachment and junction formation. *J. Exp. Med.* **149**, 172–184 (1979).
28. N. D. Geoghegan et al., 4D analysis of malaria parasite invasion offers insights into erythrocyte membrane remodeling and parasitophorous vacuole formation. *Nat. Commun.* **12**, 3620 (2021).
29. F. Wissing, C. P. Sanchez, P. Rohrbach, S. Ricken, M. Lanzer, Illumination of the malaria parasite *Plasmodium falciparum* alters intracellular pH. Implications for live cell imaging. *J. Biol. Chem.* **277**, 37747–37755 (2002).
30. M. Treeck et al., Functional analysis of the leading malaria vaccine candidate AMA-1 reveals an essential role for the cytoplasmic domain in the invasion process. *PLoS Pathog.* **5**, e1000322 (2009).

31. A. S. Yang, J. A. Boddey, Molecular mechanisms of host cell traversal by malaria sporozoites. *Int. J. Parasitol.* **47**, 129–136 (2017).
32. O. Billker, S. Lourido, L. D. Sibley, Calcium-dependent signaling and kinases in apicomplexan parasites. *Cell Host Microbe* **5**, 612–622 (2009).
33. D. A. Baker *et al.*, Cyclic nucleotide signalling in malaria parasites. *Open Biol.* **7**, 170213 (2017).
34. S. Singh, M. M. Alam, I. Pal-Bhowmick, J. A. Brzostowski, C. E. Chitnis, Distinct external signals trigger sequential release of apical organelles during erythrocyte invasion by malaria parasites. *PLoS Pathog.* **6**, e1000746 (2010).
35. H. E. Bullen *et al.*, Phosphatidic acid-mediated signalling regulates microneme secretion in *Toxoplasma. Cell Host Microbe* **19**, 349–360 (2016).
36. G. E. Weiss *et al.*, Revealing the sequence and resulting cellular morphology of receptor-ligand interactions during *Plasmodium falciparum* invasion of erythrocytes. *PLoS Pathog.* **11**, e1004670 (2015).
37. R. Joice *et al.*, *Plasmodium falciparum* transmission stages accumulate in the human bone marrow. *Sci. Transl. Med.* **6**, 244re5 (2014).
38. M. De Niz *et al.*, *Plasmodium* gametocytes display homing and vascular transmigration in the host bone marrow. *Sci. Adv.* **4**, eaat3775 (2018).
39. N. Obaldia 3rd *et al.*, Bone marrow is a major parasite reservoir in *Plasmodium vivax* infection. *MBio* **9**, 625–643 (2018).
40. B. Malleret *et al.*, *Plasmodium vivax*: Restricted tropism and rapid remodeling of CD71-positive reticulocytes. *Blood* **125**, 1314–1324 (2015).
41. K. Venugopal, F. Hentzschel, G. Valkiūnas, M. Marti, *Plasmodium* asexual growth and sexual development in the haematopoietic niche of the host. *Nat. Rev. Microbiol.* **18**, 177–189 (2020).
42. C. Zhang, The role of inflammatory cytokines in endothelial dysfunction. *Basic Res. Cardiol.* **103**, 398–406 (2008).
43. G. N. McKay, N. Mohan, N. J. Durr, Imaging human blood cells in vivo with oblique back-illumination capillaroscopy. *Biomed. Opt. Express* **11**, 2373–2382 (2020).
44. S. N. Kariuki *et al.*, Red blood cell tension protects against severe malaria in the Dantu blood group. *Nature* **585**, 579–583 (2020).
45. C. Lim *et al.*, Expansion of host cellular niche can drive adaptation of a zoonotic malaria parasite to humans. *Nat. Commun.* **4**, 1638 (2013).
46. R. W. Moon *et al.*, Normocyte-binding protein required for human erythrocyte invasion by the zoonotic malaria parasite *Plasmodium knowlesi. Proc. Natl. Acad. Sci. U.S.A.* **113**, 7231–7236 (2016).
47. W. H. Tham, J. Healer, A. F. Cowman, Erythrocyte and reticulocyte binding-like proteins of *Plasmodium falciparum. Trends Parasitol.* **28**, 23–30 (2012).
48. S. P. Wertheimer, J. W. Barnwell, *Plasmodium vivax* interaction with the human Duffy blood group glycoprotein: Identification of a parasite receptor-like protein. *Exp. Parasitol.* **69**, 340–350 (1989).
49. L. J. Chan, M. H. Dietrich, W. Nguitragool, W. H. Tham, *Plasmodium vivax* Reticulocyte Binding Proteins for invasion into reticulocytes. *Cell. Microbiol.* **22**, e13110 (2020).
50. A. V. Hoffbrand, P. A. H. Moss, *Essential Haemotology* (Wiley-Blackwell, ed. 6, 2011).
51. S. Dasgupta *et al.*, Membrane-wrapping contributions to malaria parasite invasion of the human erythrocyte. *Biophys. J.* **107**, 43–54 (2014).
52. M. L. Jones, C. Cottingham, J. C. Rayner, Effects of calcium signaling on *Plasmodium falciparum* erythrocyte invasion and post-translational modification of gliding-associated protein 45 (PfGAP45). *Mol. Biochem. Parasitol.* **168**, 55–62 (2009).
53. H. M. Kudyba, D. W. Cobb, J. Vega-Rodríguez, V. Muralidharan, Some conditions apply: Systems for studying *Plasmodium falciparum* protein function. *PLoS Pathog.* **17**, e1009442 (2021).
54. L. E. Boucher, J. Bosch, The apicomplexan glideosome and adhesins - Structures and function. *J. Struct. Biol.* **190**, 93–114 (2015).
55. D. Y. Bargieri *et al.*, *Plasmodium* merozoite TRAP family protein is essential for vacuole membrane disruption and gamete egress from erythrocytes. *Cell Host Microbe* **20**, 618–630 (2016).
56. M. Zhang *et al.*, Uncovering the essential genes of the human malaria parasite *Plasmodium falciparum* by saturation mutagenesis. *Science* **360**, eaap7847 (2018).
57. E. Knuepfer *et al.*, Divergent roles for the RH5 complex components, CyRPA and RIPR in human-infective malaria parasites. *PLoS Pathog.* **15**, e1007809 (2019).
58. W. Trager, J. B. Jensen, Human malaria parasites in continuous culture. *Science* **193**, 673–675 (1976).
59. M. Tibúrcio *et al.*, A novel tool for the generation of conditional knockouts to study gene function across the *Plasmodium falciparum* life cycle. *MBio* **10**, e01170-19 (2019).
60. F. Mohring *et al.*, Rapid and iterative genome editing in the malaria parasite *Plasmodium knowlesi* provides new tools for *P. vivax* research. *eLife* **8**, e45829 (2019).
61. M. L. Jones *et al.*, A versatile strategy for rapid conditional genome engineering using loxP sites in a small synthetic intron in *Plasmodium falciparum. Sci. Rep.* **6**, 21800 (2016).
62. T. Ishino *et al.*, Rhoptry neck protein 2 expressed in *Plasmodium* sporozoites plays a crucial role during invasion of mosquito salivary glands. *Cell. Microbiol.* **21**, e12964 (2019).
63. T. Endo, H. Tokuda, K. Yagita, T. Koyama, Effects of extracellular potassium on acid release and motility initiation in *Toxoplasma gondii. J. Protozool.* **34**, 291–295 (1987).
64. H. Fang *et al.*, Epistasis studies reveal redundancy among calcium-dependent protein kinases in motility and invasion of malaria parasites. *Nat. Commun.* **9**, 4248 (2018).